Applied Energy 140 (2015) 20–32

Contents lists available at ScienceDirect

Applied Energy

journal homepage: www.elsevier.com/locate/apenergy

# Decompression wave speed in $CO_2$ mixtures: CFD modelling with the GERG-2008 equation of state

Alhoush Elshahomi [a], Cheng Lu [a,*], Guillaume Michal [a], Xiong Liu [a], Ajit Godbole [a], Philip Venton [b]

[a] School of Mechanical, Materials and Mechatronic Engineering, University of Wollongong, Wollongong, NSW 2522, Australia
[b] Venton and Associates Pty. Ltd., Bundanoon, NSW 2578, Australia

## HIGHLIGHTS

- CFD models for decompression simulation of $CO_2$ mixtures.
- Incorporation of GERG-2008 EOS into CFD code for decompression modelling.
- Predicted decompression wave speed validated by measurements.
- Studies of effects of initial temperature and impurities on decompression wave speed.

## ARTICLE INFO

*Article history:*
Received 19 May 2014
Received in revised form 16 October 2014
Accepted 23 November 2014
Available online 12 December 2014

*Keywords:*
$CO_2$ pipeline
Decompression wave speed
Equation of state
Computational Fluid Dynamics
Fracture propagation arrest

## ABSTRACT

The development of $CO_2$ pipelines for Carbon Capture and Storage (CCS) raises new questions regarding the control of ductile fracture propagation and fracture arrest toughness criteria. The decompression behaviour in the fluid must be determined accurately in order to estimate the proper pipe toughness. However, anthropogenic $CO_2$ may contain impurities that can modify the fluid decompression characteristics quite significantly. To determine the decompression wave speed in $CO_2$ mixtures, the thermodynamic properties of these mixtures must be determined by using an accurate equation of state. In this paper we present a new decompression model developed using the Computational Fluid Dynamics (CFD) package ANSYS Fluent. The GERG-2008 Equation of State (EOS) was implemented into this model through User Defined Functions (UDF) to predict the thermodynamic properties of $CO_2$ mixtures. The model predictions were in good agreement with the experimental data of two 'shock tube' tests. A range of representative $CO_2$ mixtures was examined in terms of the changes in fluid properties from the initial conditions, with time and distance, immediately after a sudden pipeline opening at one end. Phase changes that may occur within the fluid due to condensation of 'impurities' in the fluid were also investigated. Simulations were also conducted to examine how the initial temperature and impurities would affect the decompression wave speed.



## 1. Introduction

The burning of fossil fuels and biomass continues to be the main source of energy worldwide [1,2]. Such processes emit significant quantities of Green House Gases (GHG), particularly Carbon Dioxide ($CO_2$), which has been identified as the major contributor to global warming and climate change [3,4]. Carbon Capture and Storage (CCS) technology was introduced as a key $CO_2$ abatement option to mitigate emissions of GHG by 50% by 2050, while populations and economies are expected to continue to grow globally [5]. This technology will necessitate substantial quantities of $CO_2$ to be conveyed, predominantly by pipelines, over long distances from source to storage sites [6]. In terms of operational and economic motivations, the best way to transport $CO_2$ mixtures via pipes will be in a liquid and/or supercritical state because a purely gaseous phase transmission would necessitate significantly larger diameter pipelines for the same mass flow rate [7,8]. Under these operational conditions, the possibility of running fractures in the pipeline is a major concern, so arresting and/or preventing them is important for the integrity and safety of the pipeline's operation [5,7].

Fracture propagation in gas pipelines is commonly treated using the semi-empirical Battelle Two-Curve Model (BTCM) [9,10] where the aim is to estimate the required toughness to arrest crack propagation. This method involves the superposition

* Corresponding author. Tel.: +61 2 4221 4639; fax: +61 2 4221 5474.
*E-mail address:* chenglu@uow.edu.au (C. Lu).

http://dx.doi.org/10.1016/j.apenergy.2014.11.054
0306-2619/

**Nomenclature**

| | |
|---|---|
| $c$ | speed of sound (m s$^{-1}$) |
| $E$ | fluid energy (kJ) |
| $h$ | enthalpy (kJ kg$^{-1}$) |
| $M$ | molecular weight (kg) |
| $p$ | pressure (Pa) |
| $s$ | entropy (kJ kg$^{-1}$ K$^{-1}$) |
| $t$ | time (s) |
| $T$ | temperature (K) |
| $u$ | outflow velocity (m s$^{-1}$) |
| $P_i$ | initial pressure (Pa) |
| $T_i$ | initial temperature (K) |
| $Vc$ | fracture velocity (m s$^{-1}$) |
| $W_{ave}$ | average decompression wave speed (m s$^{-1}$) |
| $W_{exp}$ | measured decompression wave speed (m s$^{-1}$) |
| $W_{local}$ | local decompression wave speed (m s$^{-1}$) |
| $k_{eff}$ | effective thermal conductivity (W m$^{-1}$ K$^{-1}$) |
| $c_p$ | specific heat (kJ kg$^{-1}$ K$^{-1}$) |
| $\rho$ | fluid density(kg m$^{-3}$) |
| $v_x$ | axial velocity (m s$^{-1}$) |
| $v_y$ | radial velocity (m s$^{-1}$) |
| $\mu$ | dynamic viscosity (Pa s) |

*Abbreviations*

| | |
|---|---|
| 2D | two-dimensional |
| AGA | American Gas Association |
| AS | Australian Standard |
| AUSM | Advection Upstream Splitting Method |
| BTCM | Battelle Two-Curve Model |
| BWRS | Benedict–Webb–Rubin–Starling |
| CCS | Carbon Capture and Storage |
| CFD | Computational Fluid Dynamics |
| $CO_2$ | Carbon dioxide |
| CVN | Charpy V-Notch |
| EOS | equation of state |
| FDM | Finite Difference Method |
| FVM | Finite Volume Method |
| GERG | Groupe Européen de Recherches Gazières |
| GHG | Green House Gases |
| ID | internal diameter |
| UDF | User Defined Functions |
| MOC | Method of Characteristics |
| PR | Peng–Robinson |
| RKS | Redlich–Kwong–Soave |

of two independently determined curves: the fluid decompression wave speed and the fracture propagation speed (the 'J curve'), each expressed as a function of pressure. Fig. 1 shows a schematic representation of the BTCM. The shape of the fluid decompression wave speed curve depends on the phase of the fluid, as shown by the red and green curves in Fig. 1. Curves 1, 2, and 3 represent the fracture speed curves for different toughness values.

When fracture curves 2 and 3 intersect with the two-phase decompression characteristic, the fracture and the gas decompression wave move at the same speed, but here the gas pressure at the tip of the fracture no longer decreases, implying that the fracture will continue to propagate. The boundary between arrest and propagation of a running fracture is represented by tangency between the gas decompression wave speed curve and the fracture speed curve (curve 1 with the two-phase decompression wave speed curve and curve 3 with the single phase decompression wave speed curve). According to the BTCM, the minimum toughness required to arrest the propagation of fracture is the value of toughness corresponding to this tangency condition [9,11].

Several numerical models have been proposed to predict the decompression wave speed, mainly in natural gas mixtures. One of these models is GASDECOM [12]. This model uses an analytical

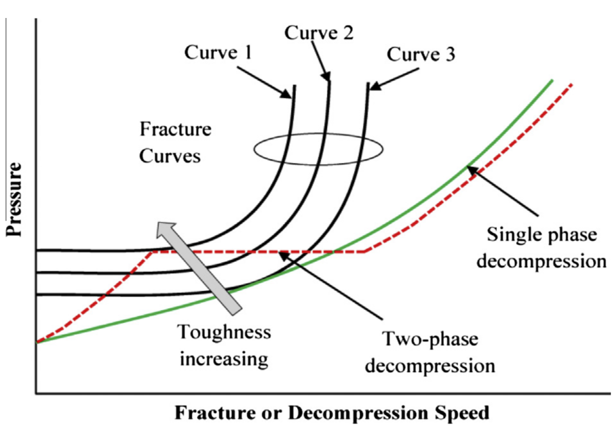


**Fig. 1.** Schematic of the BTCM [11].

expression for the propagation of an infinitesimal decompression front to determine the decompression wave speed. The main assumptions in such models include: one-dimensional, frictionless, isentropic, and homogeneous-equilibrium fluid flow. GASDECOM uses the Benedict–Webb–Rubin–Starling (BWRS) equation of state (EOS) [13] with modified constants to estimate the thermodynamic properties during isentropic decompression. GASDECOM has suffered from numerical instabilities when dealing with mixtures containing higher fractions of $CO_2$. It should be mentioned that the instabilities are due to the implementation in the code, and are not fundamental. GASDECOM cannot be used for mixtures containing hydrogen, oxygen and argon, which are often mixed with $CO_2$ in CCS-related operations. This is because these components were not originally included in the BWRS EOS [14,15]. Several other models also use assumptions similar to GASDECOM [16], and only differ in the choice of EOS. DECOM [17] was developed to predict the decompression wave speed in $CO_2$ mixtures, and is also based on assumptions similar to those in GASDECOM. The only difference was use of the NIST Standard Reference Database 23 (REFPROP version 9.0) [18], along with the built-in Span and Wagner EOS [19] for pure $CO_2$ and the GERG-2004 EOS [20] for multi-component $CO_2$ mixtures.

Other more complex decompression models that can account for non-isentropic effects using the Computational Fluid Dynamics (CFD) technique have been developed. Examples include: Picard and Bishnoi [21,22], PipeTech [23,24] and CFD-DECOM [25]. These are based entirely on assumptions of one-dimensional homogeneous-equilibrium fluid flow. In these models the effects of friction, heat transfer, and pipe diameter can be considered, which is particularly relevant for smaller diameter and longer pipelines where friction could lead to a range of complex effects on local flow conditions, temperature, and pressure within the pipeline [24,26–29]. CFD-based techniques involve discretising the governing partial differential equations of fluid flow. The Finite Difference Method FDM [30,31], the Method of Characteristics (MOC) [32], and the Finite Volume Method (FVM) [25] are examples of discretisation methods. The MOC solves the fluid flow conservation equations by following the Mach-line characteristics inside the pipe. It is claimed that numerical diffusion related to the finite difference approximation of partial derivatives is reduced by this method [33,34], but the MOC needs much longer computation runtimes and cannot predict non-equilibrium or heterogeneous flows [25,35], while the FVM is better at dealing with multi-dimensional flow. In the existing CFD models, the cubic Peng–Robinson (PR) EOS [36] is often used due to its relatively simple mathematical form compared to other more complex (but more accurate) EOS such as AGA-8 [37], BWRS [13] and GERG [20].

To accurately predict the decompression behaviour of $CO_2$ mixtures, accurate means of predicting the thermodynamic properties of these mixtures using accurate EOS is essential. To date, no EOS is specifically recommended for $CO_2$ mixtures, but the ability to accurately predict the Vapour Liquid Equilibrium (VLE), density and speed of sound is considered the best way to gauge any weaknesses or strengths of EOS [2,8,38,39]. Li et al. [2,8] have evaluated eight cubic EOS, including Peng–Robinson (PR) [36], Patel–Teja (PT) [40], Redlich–Kwong (RK) [41], Redlich–Kwong–Soave (SRK) [42], modified SRK (MRK) [43], modified PR (MPR) [44], 3P1T EOS [45], and Improved SRK (ISRK) [46], in terms of predicting the VLE and specific volumes of binary $CO_2$ mixtures containing $CH_4$, H2S, $SO_2$, Ar and $N_2$, based on the comparisons with experimental data. Generally, PR is recommended for calculations involving $CO_2$/$CH_4$ and $CO_2$/$H_2S$; PT is recommended for $CO_2$/$O_2$, $CO_2$/$N_2$ and $CO_2$/Ar; 3P1T is recommended for $CO_2$/$SO_2$. Liu et al. [47] have implemented the PR EOS into ANSYS Fluent using real gas User-Defined Functions (UDFs) in order to simulate the dispersion of pure $CO_2$ releases from high-pressure pipelines. Reasonable results were obtained when using the real gas models in conjunction with the CFD method. Botros [48,49] conducted a comparative study of five different EOSs: GERG, AGA-8, BWRS, PR and Redlich–Kwong–Soave (RKS) and compared the predicted densities in the dense phase region using those EOS with measured values for different hydrocarbon mixtures. It was determined that the GERG EOS outperformed the other EOS in the region up to $P = 30$ MPa and $T > -8$ °C. However, the GERG EOS has not been implemented in CFD models of decompression or outflow models to date, though it is currently the reference EOS for natural gas [50].

In this paper we present a CFD model for a full-bore depressurisation of a $CO_2$ mixture pipeline developed using the versatile CFD software ANSYS Fluent (v 14.5). The built-in EOS in ANSYS Fluent cannot predict the fluid properties of $CO_2$ mixtures accurately. The GERG-2008 EOS was successfully implemented into ANSYS Fluent to accurately predict the thermodynamic properties of $CO_2$ mixtures, for the first time. The method used to implement the GERG-2008 EOS into ANSYS Fluent is described. The results were validated against experimental data from two separate 'shock tube' tests, and a number of simulations were also conducted to examine the effect of different initial conditions and different components in the $CO_2$ mixture.

## 2. Methodology

The CFD package ANSYS-Fluent was used to develop the CFD decompression model because it satisfies the three main demands required for gas decompression analysis:

- Ability to solve transient flows.
- Possibility of invoking an accurate EOS through user-defined subroutines.
- Ability to handle multi-dimensional geometries.

### 2.1. Computational domain and boundary conditions

The physical flow domain in the shock tube tests consisted of the initially pressurised gas in a horizontal pipe, which undergoes a 'full-bore' opening at one end using a rupture disc as schematically depicted in Fig. 2. The axial symmetry made it possible to construct a two-dimensional computational domain and thus reduce the computational runtime.

The following assumptions are made to develop this model: unsteady, two-dimensional flow; the rupture is instantaneous and represented by a full bore opening, non-isentropic flow conditions (the friction effect is considered); the gas velocity before the rupture of the pipe is negligible compared with the conditions post-rupture; the fluid is considered homogenous so equilibrium conditions prevail during condensation; and the 'no slip' condition is satisfied at the pipe wall.

Four boundary conditions were defined: two 'wall' boundaries defined at the top ($y = D/2$) and the end ($x = L$) of the computational domain; a 'symmetry' boundary (at $y = 0$) on the axis and a pressure outlet (zero gauge pressure) to model the rupture disk (sudden opening to the ambient) at $x = 0$. Based on the above assumptions, the unsteady, two-dimensional form of the governing differential equations of conservation of mass, momentum and energy are solved in this model.

### 2.2. Numerical method

The FVM is used in ANSYS Fluent to discretise the fluid conservation equations. The implicit first order spatial and temporal formulations were used with the Advection Upstream Splitting Method (AUSM) for the density-based solver [51]. This solver is designed for high-speed compressible flows and allows the use of a user defined real gas model. The governing flow equations of mass, momentum, and energy conservation, supplemented by the auxiliary equation (i.e. EOS) were solved simultaneously while the turbulence equations were treated sequentially. In the density-based solver, the momentum equations were used to obtain the velocity field, while the continuity equation was used to determine the density field and the pressure field was determined from the EOS.

The computational grid conformed to the physical dimensions of the shock tube used in the tests. A 'symmetry' boundary condition was used on the axis. At the rupture end ($x = 0$), the fluid was considered to be exposed to ambient pressure at time $t = 0+$. A no-slip wall was set as the boundary condition for the closed end of the pipe and the pipe wall. Adjacent to both wall boundaries 5 cells were generated to span the boundary layer. The cell adjacent to the wall and the outlet was set at 0.05 mm from the wall with a mesh-growth factor of 1.25. Beyond the 5th cell, the dimensions of the cells ($\Delta x$) and ($\Delta y$) remained constant at 2 mm in both axial and radial directions. The initial conditions for the flow variables were prescribed based on the operating conditions of each shock tube test whereas the time step size was fixed to $1e^{-6}$ s. The above mesh and time step size were the best setting to obtain an accurate and converged solution. A detail of the mesh near the outlet is shown in Fig. 3.

The speed of the decompression wave was obtained by first calculating the *local* decompression wave speed using Eq. (1), i.e., by monitoring the speed of sound '$c$' and the 'outflow' velocity '$u$' against time during the decompression process. The decompression wave speed was then determined by subtracting the outflow velocity from the speed of sound for several pressures below the initial pressure.

$$W_{local} = c - u \tag{1}$$

However, experimental tests such as the shock tube test did not provide the *local* gas decompression wave speed directly because the gas decompression wave speed $w$ was calculated by determining the times at which a certain pressure level was recorded at several pressure transducers at known locations on the pipe wall. By plotting these locations against time, the decompression wave speed was obtained by performing a linear regression of each

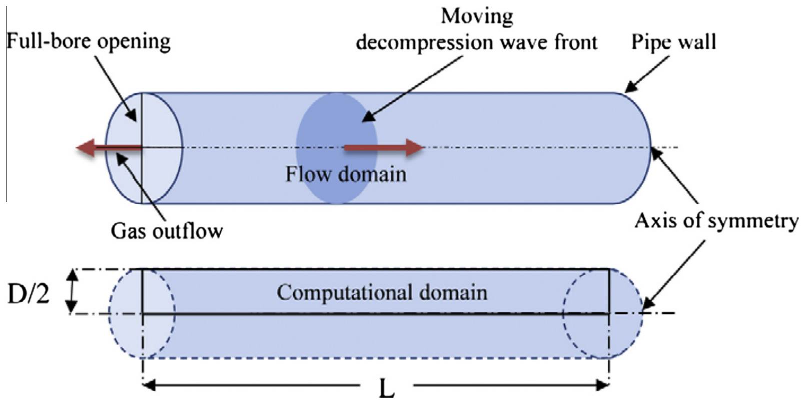


**Fig. 2.** Flow domain and computational domain – schematic.

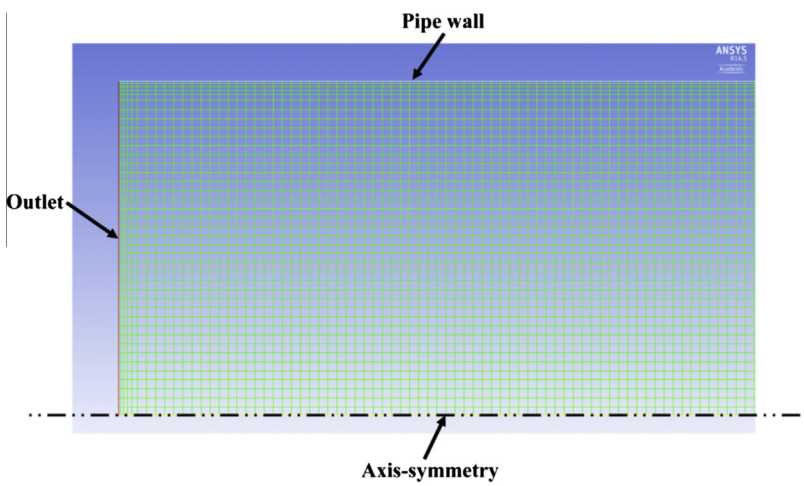


**Fig. 3.** Two-dimensional computational grid.

isobar curve. The slope of each regression represents the average decompression wave speed for each isobar.

$$W_{ave} = \frac{dx}{dt} \tag{2}$$

## 3. Implementation of GERG-2008 EOS into ANSYS fluent

To simulate the real behaviour of gas flow, the thermodynamic properties must be predicted using an accurate real gas EOS. The modern multi-component GERG-2008 EOS [20,52] was used to provide the thermodynamic properties of $CO_2$ mixtures. This EOS covers the gas phase, liquid phase, supercritical region, and vapour-liquid equilibrium states for mixtures consisting of up to 21 components: *methane, nitrogen,* ***carbon dioxide****, ethane, propane, n-butane, isobutane, n-pentane, isopentane, n-hexane, n-heptane, n-octane, hydrogen, oxygen, carbon monoxide, water, helium, argon, n-nonane, n-decane, and hydrogen sulphide*. The normal range of validity of this EOS covers temperatures from 90 K to 450 K and pressures up to 35 MPa. Currently, GERG-2008 EOS is considered to be a reference EOS for natural gas pipelines [14].

The GERG-2008 EOS must be implemented in Fluent using a User-Defined Real Gas Model (UDRGM) using a library of functions written by the end user in the C programming language. These functions represent several thermodynamic properties required by Fluent to solve the system of governing equations. The thermodynamic properties required for Fluent calculation are shown in Table 1.

These properties were supplied to Fluent for given values of pressure and temperature, but because GERG-2008 cannot be programmed within the UDF, the exported functions and subroutines of the dynamic link library 'GERG-2008.DLL' [52] had to be defined within UDF instead. The EOS library is called to calculate the properties at each node in the flow domain. The cost of a direct call to the library during simulation can be a major limitation, and occasionally the library failed to produce some properties at certain P-T values and entered an infinite optimisation loop that caused the library to crash. Moreover, some properties (e.g. speed of sound) were not defined in the two-phase region, so an error was reported. Most modern multi-component EOSs suffer from this drawback. The most frequent error encountered during the simulated decompression was related to the speed of sound in the

**Table 1**
Thermodynamic properties required for a real gas model in ANSYS Fluent.

| Property | Symbol |
|---|---|
| Density | $\rho$ |
| Enthalpy | $h$ |
| Entropy | $s$ |
| Speed of sound | $c$ |
| Specific heat at constant pressure | $c_p$ |
| Molecular weight | $M$ |
| Partial derivative of $\rho$ w.r.t. $T$ | $\partial\rho/\partial T$ |
| Partial derivative of $\rho$ w.r.t. $P$ | $\partial\rho/\partial P$ |
| Partial derivative of $h$ w.r.t. $P$ | $\partial h/\partial P$ |

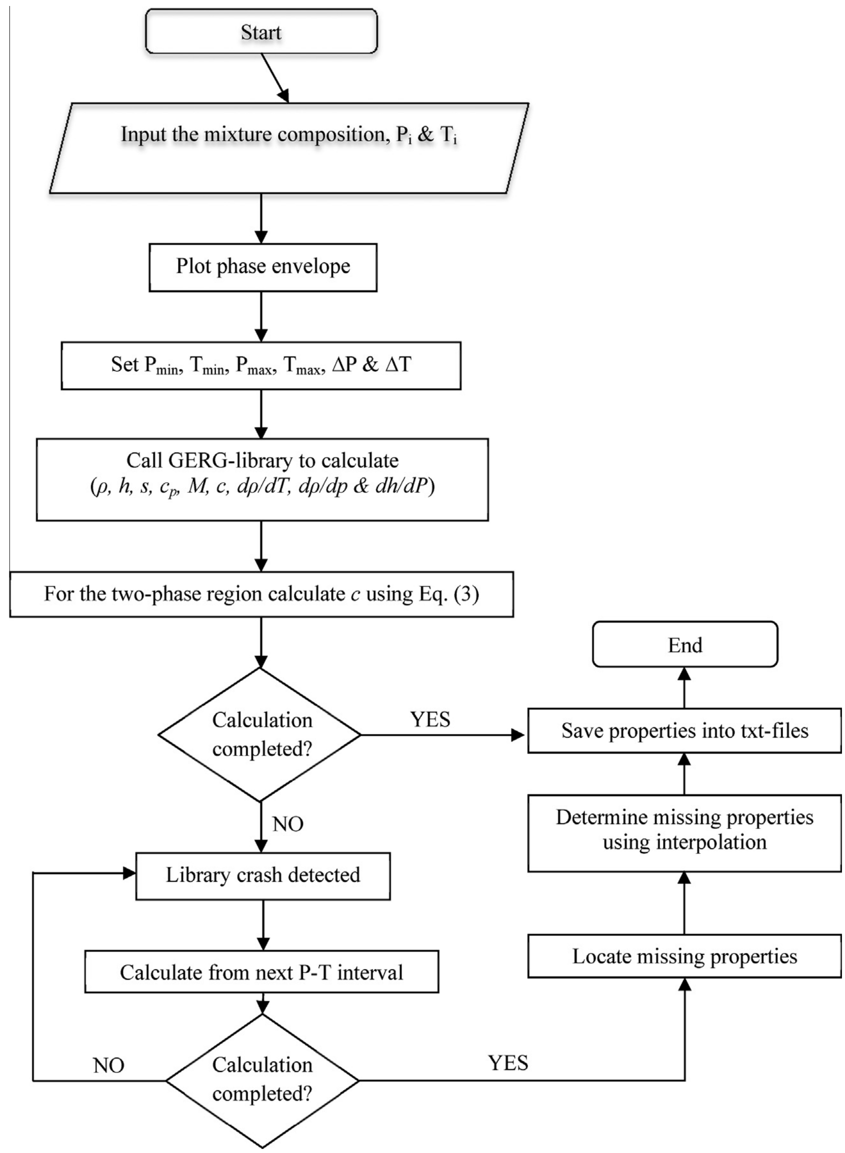


**Fig. 4.** Property calculation flow chart.

two-phase region. In this model we assumed a homogenous-equilibrium fluid, so the definition of the speed of sound for a single phase fluid could be used in the UDF to overcome the problem. The speed of sound in the two-phase region was defined as:

$$c = \sqrt{\left.\frac{dp}{d\rho}\right|_s} \tag{3}$$

Despite not always being able to calculate the requested property, the above obstacles did not mean the decompression wave velocity could not be accurately predicted. We circumvented those issues by using the EOS library indirectly such that reference to pre-compiled tables of the relevant thermodynamic properties generated by the GERG-2008 EOS replaced a direct call to the dynamic link library 'GERG-2008.DLL [53]'. A linear interpolation scheme was also implemented within the UDF to extract values of the other thermodynamic parameters based on the *P–T* values solved for by Fluent. This method has proved to be 300 times faster than direct calls to EOS [54] and could save up to 70% of the total computational run time [55]. In this study the performance of the UDF was tested using both methods and for all properties, the search in tables during the simulation was found to be about 20 times faster than a direct call to the library.

A structured two-dimensional array for the chosen ranges of pressures and temperatures was established. The initial conditions and the phase envelope were the key parameters used to establish the boundary of the main *P–T* table. The EOS library was called for each pressure–temperature node in the 2D-table to produce tables of the properties listed in Table 1. Where the EOS library failed to produce data, hole(s) were displayed in the corresponding table cell(s) and a code was developed to begin the calculation from the next *P–T* increment and complete the rest of the tables so the remaining properties were displayed normally. The corresponding gaps in the table grid were then filled using interpolation based on the values at the neighbouring nodes. The calculated properties were then saved into readable files linked to ANSYS Fluent through the UDF as *LOOK-UP* tables. Fig. 4 shows schematically the computing strategy of fluid properties using the GERG-2008 library.

## 4. Model results and validation

The following paragraphs present the results of the 2D CFD decompression model using the GERG-2008 EOS. This model was validated by a comparison with the results of two separate shock tube tests. The first test (Case A) was conducted at the TransCanada

**Table 2**
Model parameters setting for the current study.

| Case | Pipe length (m) | Diameter (mm) | Surface roughness (μm) | Turbulence model |
|---|---|---|---|---|
| Case A | 42 | 38.1 | Smooth | Realisable $k$–$\varepsilon$ |
| Case B | 144 | 146.36 | 5 | Realisable $k$–$\varepsilon$ |

pipeline Gas Dynamics Test Facility in Didsbury, Alberta, Canada [56]. The second test (Case B) was commissioned by the National Grid at GL Noble Denton's Spadeadam Test Site in Cumbria, UK [17]. In the first test, the main section of the shock tube was 42 m long, the internal diameter (ID) was 38.1 mm and the tube wall thickness was 11.1 mm. In the second test the pipe was 144 m long, the ID was 146.36 mm, and the pipe wall thickness was 10.97 mm. In Case A, a 'smooth' pipe surface was used, while in Case B the pipe has an average surface roughness ranging between 5 and 6.3 μm. The smoothest pipe was placed nearest the rupture disk. Table 2 lists model parameters used in the current simulations.

CFD simulations were carried out for two mixtures: a binary mixture for Case A and a 5-component mixture for Case B. Table 3 shows the gas compositions and initial conditions of the two tests.

A mesh-dependence study was carried out for both cases using several element sizes (2, 3, 5, 10, 20, 50, 100 mm). An optimum element size was found to be 2 mm, although for decompression wave speed calculation, an element size up to 10 mm was found acceptable.

The pressure and temperature were monitored as a function of time at several locations along the axial direction, near the exit plane. These locations corresponded to where the pressure transducers and temperature probes were in the shock tubes tests. Other properties such as the speed of sound and 'outflow' velocity were monitored at the same locations to determine the local decompression wave speed. Table 4 shows the locations of pressure and temperature transducers mounted on both shock tube tests. The highlighted cells in Table 4 represent locations used for the determination of decompression wave speed.

The thermodynamic properties of each mixture were first produced using the GERG-2008 EOS and then saved into readable files. Table 5 shows the structure of the $P$–$T$ table established for the mixture in Case A. The properties were calculated for all $P$–$T$ nodes in the Table. Note that the minimum and maximum values of $P$ and $T$ in the main table will vary depending on the initial conditions and phase envelope of each mixture.

A MATLAB code was written to generate plots of the required properties as a function of pressure and temperature. The calculated properties for Case A are presented in Fig. 5. A smooth distribution was observed for all properties, including the region under the two-phase boundary. This occurred because the main $P$–$T$ table was made dense enough to account for changes near the phase boundary. This makes for very large files, but it ensured that the calculations were accurate. An acceptable accuracy was achieved using the property tables: the interpolated properties deviated from values obtained directly using the EOS library by approximately 0.001% outside the two-phase region, and 0.1% within the two-phase region.

**Table 4**
Monitor point locations.

| TEST 1 (Case A) | | TEST 2 (Case B) | |
|---|---|---|---|
| Location | Distance from rupture disc (m) | Location | Distance from rupture disc (m) |
| *PT1* | *0.0295* | P2 | 0.0864 |
| PT1A | 0.0924 | *P4, T4* | *0.34* |
| PT1B | 0.1028 | *P6* | *0.54* |
| *PT2* | *0.2* | *P8* | *0.74* |
| *PT3* | *0.35* | *P10* | *0.94* |
| PT4 | 0.5 | *P12* | *1.24* |
| *PT5* | *0.7* | *P14, T14* | *1.84* |
| *PT6* | *0.9* | *P16* | *2.44* |
| *PT7* | *1.1* | *P18* | *3.64* |
| PT8 | 3.1 | P19 | 4.84 |
| PT9 | 5.1 | T20 | 6.04 |
| PT10 | 7.1 | P21 | 9.04 |
| PT11 | 9.1 | P22 | 13.54 |
| PT12 | 13 | T23 | 18.04 |
| PT13 | 19 | P24 | 22.54 |
| PT14 | 25 | T25 | 30.04 |

**Table 5**
$P$–$T$ table.

| | Pressure (MPa) | Temperature (K) |
|---|---|---|
| Min | 0.05 | 180 |
| Max | 30 | 320 |
| Increment | 0. 1 | 0.5 |
| No. of nodes | 300 | 281 |

Decompression of the mixture in Case A was simulated first, with a flow domain compatible with the shock tube test described in [56]. As Fig. 6 shows, the simulated pressure–time histories compared well with the measurements at different points near the exit, but as the decompression wave front reached each location, the pressure at each point dropped rapidly before levelling off at about 9 MPa. There was a slight discrepancy between the measured and predicted pressure at pressures between 27 and 26 MPa. Apart from that, the predicted change in pressure agreed satisfactorily with the experimental results.

Fig. 7 shows the transient behaviour of the fluid temperature at the four locations closest to the outlet boundary (rupture disc). The variations in the speed of sound and the outflow velocity are shown in Fig. 8 and Fig. 9 respectively. The forms of the pressure–time and temperature–time curves were similar. The fluid temperature suddenly dropped from its initial value to 276 K. The temperature remained steady at this value for several time steps, creating a temperature plateau, before continuing to drop steadily.

The predicted speed of sound at the initial conditions was 516.28 m/s. Fig. 8 shows that the speed of sound gradually decreased to a value close to 258 m/s and then dropped to their lowest level of 105 m/s.

Before the rupture disk ruptured, the entire body of gas in the pipeline was at rest. In the simulation, as the outlet

**Table 3**
Mixture composition and initial conditions of shock tube tests.

| Shock Tube Test | Mixture components (mole %) | | | | | $P_i$ (MPa) | $T_i$ (K) |
|---|---|---|---|---|---|---|---|
| | $CO_2$ | $H_2$ | $N_2$ | $O_2$ | $CH_4$ | | |
| Case A | 72.6 | 0 | 0 | 0 | 27.4 | 28.568 | 313.65 |
| Case B (T31) | 91.03 | 1.15 | 4 | 1.87 | 1.95 | 14.95 | 283.15 |

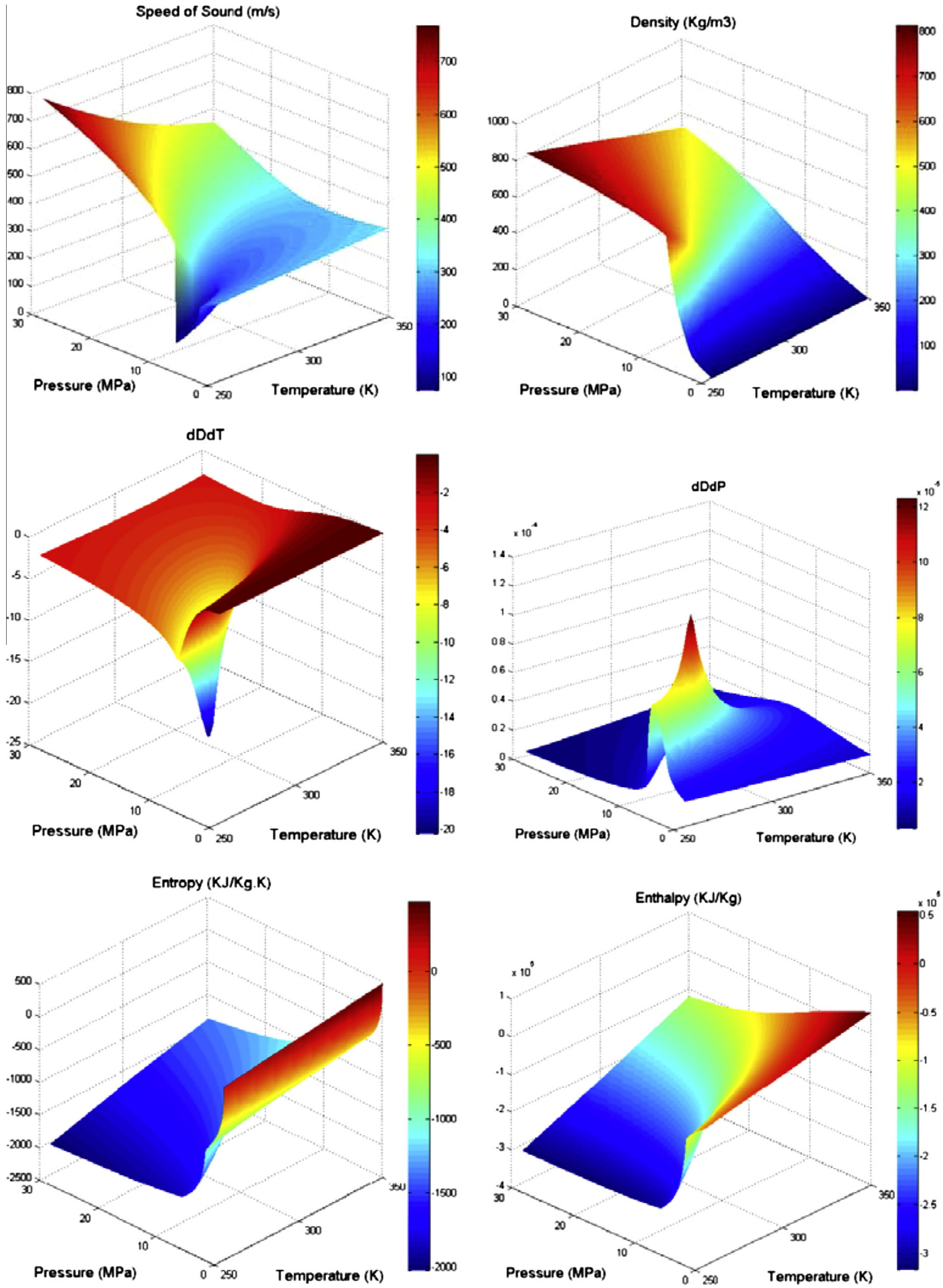


**Fig. 5.** 3-D plots of thermodynamic properties calculated by GERG-2008 (Case A).

boundary was subjected to ambient pressure at time $t = 0+$, an expansion (decompression) wave was set off. As the wave propagated away from the opening, the exit velocity was seen to increase. Like the other properties, the outlet velocity remained steady for a short time at 85 m/s before continuing to increase again.

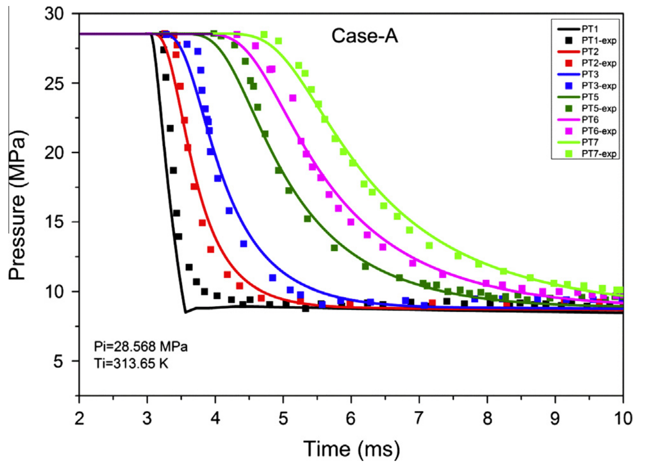


**Fig. 6.** Comparison between predicted and measured pressure–time traces (Case A).

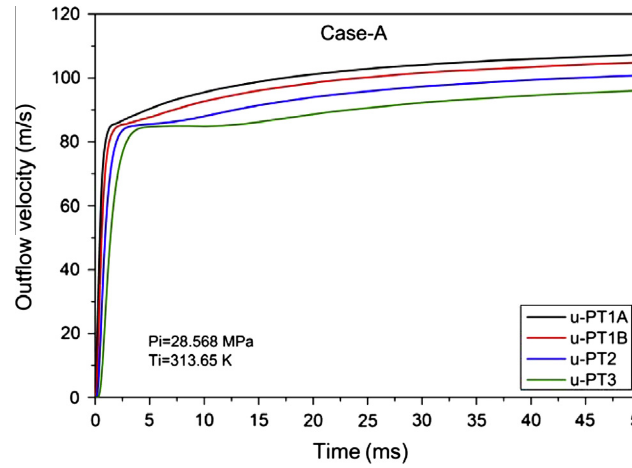


**Fig. 9.** Predicted 'outflow' velocity versus time (Case A).

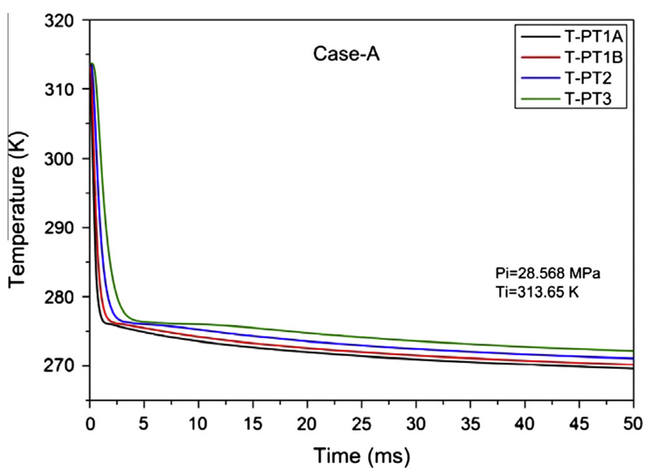


**Fig. 7.** Predicted fluid temperature versus time (Case A).

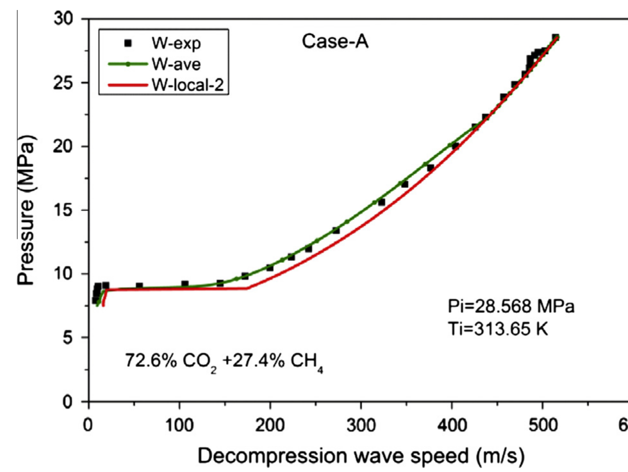


**Fig. 10.** Comparison of the predicted and the measured decompression wave speed (Case A).

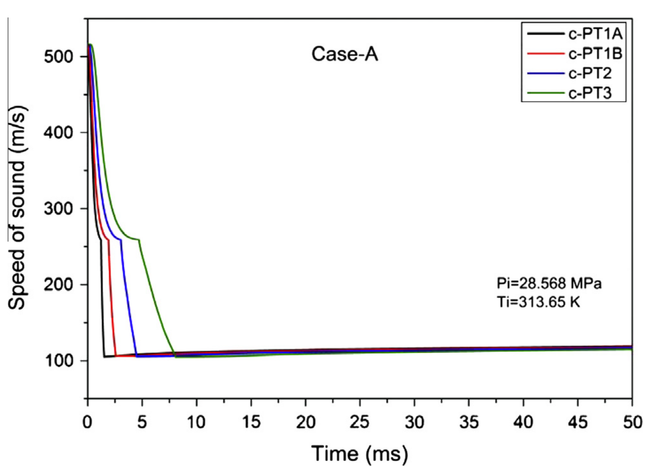


**Fig. 8.** Predicted speed of sound vs time (Case A).

Fig. 10 shows a comparison between the predicted and experimentally obtained decompression wave speed. The predicted *average* decompression wave speed was obtained based on readings at the 6 pressure transducers listed in Table 3, whereas the *local* decompression wave speed was determined using the predicted speed of sound and the 'outflow' velocity at 200 mm from the exit. Initially (before the flow commenced), the speed of the decompression wave was equal to the predicted speed of sound in the mixture because the 'outflow' speed was zero. The model predicted the initial decompression wave speed well, differing by only 0.4% from the measured data. As the pressure decreased the predicted average decompression wave speed agreed with the measured data, while the local decompression wave speed varied slightly to the right of the experimental curve because the 'local' decompression wave speed was obtained using the formulation in Eq. (1), while the average decompression wave speed was calculated using a similar approach to the measured data (based on the pressure–time traces).

More importantly, the abrupt drop in the measured decompression wave speed curve which created a long pressure plateau was predicted successfully. According to the BTCM, an accurate determination of the pressure plateau in the decompression wave speed curve is crucial to guarantee an accurate prediction of the required arrest toughness. The current model under-predicted the plateau level slightly. As seen in Fig. 6, a discrepancy is noticed on the predicted pressure–time curves at the same pressure level. The reason for the discrepancy and its influence is discussed later.

The appearance of the plateau can be explained by superimposing the pressure–temperature gradient on the phase envelope as depicted in Fig. 11. As the fluid crosses the phase boundary (at

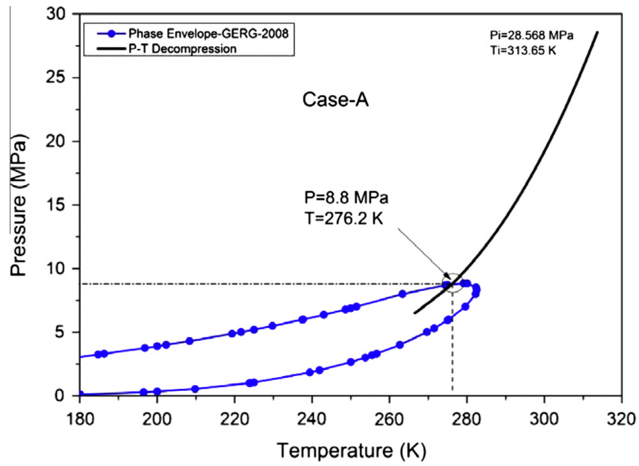


**Fig. 11.** The pressure–temperature curve and the phase envelope (Case A).

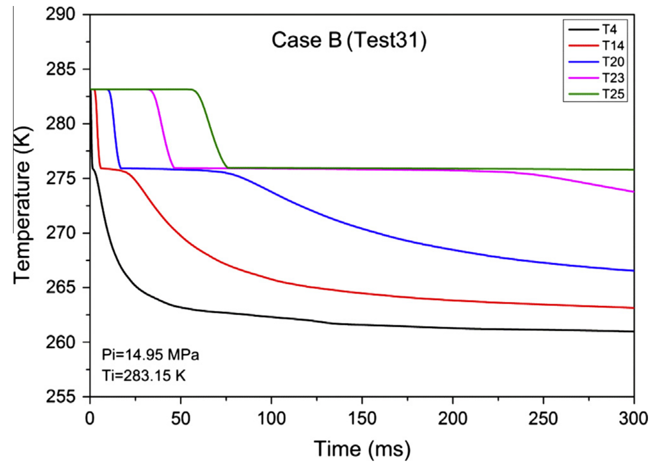


**Fig. 13.** Predicted temperature–time traces (Case B).

$T = 276$ K, $P = 8.8$ MPa), the decompression wave speed experiences a sharp drop which can be attributed to the drop in the speed of sound, while simultaneously the monitored properties remained constant for several time steps. Clearly, the trend that appeared in all properties stemmed from the discontinuity at the phase boundary. Such outcomes demonstrate that the current CFD model can successfully deal with the phase change predicted implicitly in the property tables.

The second simulation was for the mixture in Case B. The computational domain here was based on the physical dimensions of the shock tube test described in [17]. Fig. 12 shows the CFD prediction of pressure–time traces at 8 different pressure transducer locations along the pipe. A rapid drop in pressure occurred as the decompression wavefront passed each location. The appearance of a plateau at about 8 MPa can be ascribed to the phase change that occurred due to the decompression process.

Fig. 13 shows the drop in fluid temperature as a function of time at five different locations on the tube. The temperature dropped rapidly from its initial value before flattening out for several time steps at 277 K, creating a plateau in all curves. After this stage, the temperature steadily decreased to its lowest value of 260 K which is predicted at the closest location towards the rupture disc. A comparison with Fig. 14 shows that the plateaus occurred at the

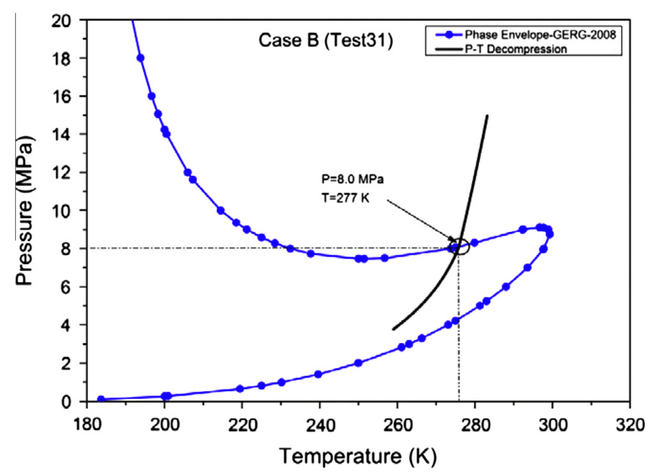


**Fig. 14.** The decompression of pressure–temperature compared to phase envelope (Case B).

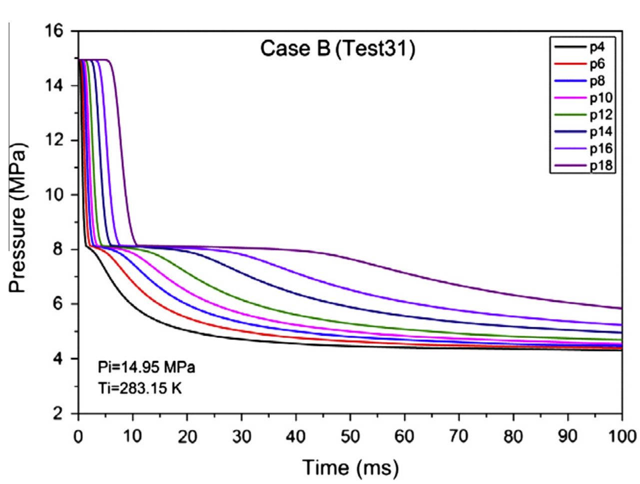


**Fig. 12.** Predicted pressure–time traces (Case B).

same pressure level as the point of intersection of the pressure–temperature curve with the phase boundary.

The speed of sound and the outflow velocity were both predicted in order to obtain the local decompression wave speed. The predicted speed of sound versus time for five locations close to the outlet is shown in Fig. 15, while the predicted outflow velocity is shown in Fig. 16. At the initial pressure and temperature, the current model predicted the speed of sound as 522 m/s, while the outflow velocity was 0 m/s anywhere inside the tube (before flow commenced). A similar trend that occurred in the outflow velocity of Case A occurred here where a kink appeared on all the curves due to phase change. Referring back to the speed of sound curves, the phase change caused a decrease in the speed of sound, and this overall drop in speed of sound due to discontinuity at the phase boundary was ~350 m/s.

Fig. 17 shows a comparison between the predicted and experimentally obtained decompression wave speed of Case B where the initial decompression wave speed predicted by the current model was 521 m/s. This value deviated by approximately +2.4% from the measured result, but the predicted decompression wave speed was consistent with the experimentally obtained value for pressure levels above and below the plateau level. At the plateau there was a discrepancy between the predicted and measured decompression wave speed even though the plateau began to form close

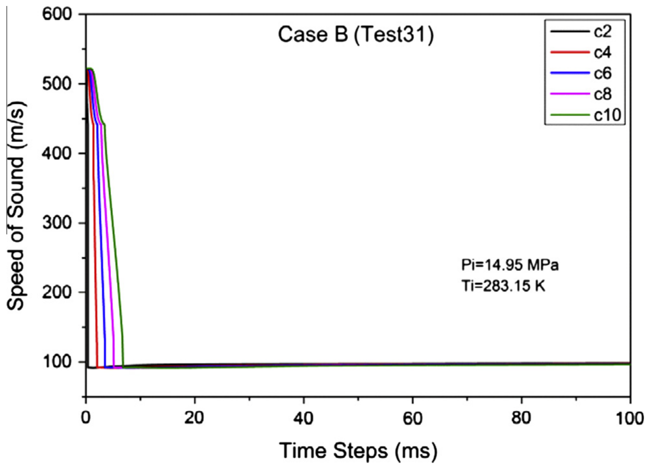


**Fig. 15.** The predicted speed of sound versus time (Case B).

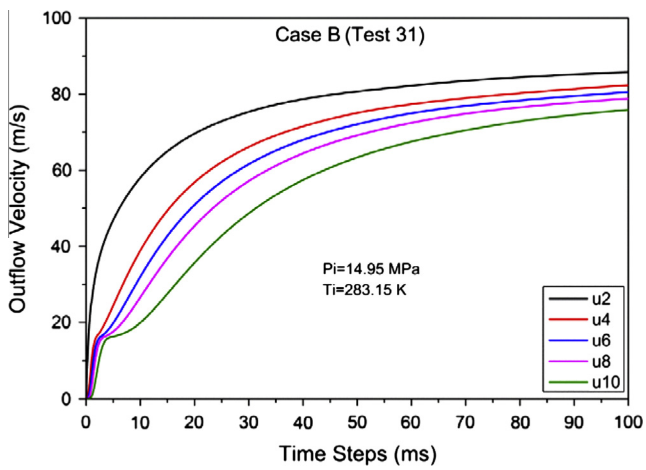


**Fig. 16.** The predicted outflow velocity versus time (Case B).

to the pressure level of the measured data. Notably, the length of the predicted plateau in the average decompression wave speed curve was consistent with the measured data. Further discussion will be made hereafter.

## 5. Discussion

If the variation in the simulated pressure matches the experimental results (Fig. 6), the predicted average value of the decompression wave speed $W$ should agree with the measured curve (Fig. 10), but as Fig. 10 shows, there was a slight discrepancy at the plateau between the predicted and experimentally obtained decompression wave speed. This variation appeared at the same pressure levels on the pressure–time curves, as Fig. 6 shows. There was major difference at the plateau level on the decompression wave speed in the second case, as Fig. 17 shows. Such a variation may result from uncertainties inherent in the numerical method and/or the way of implementing the GERG-2008 EOS, although factors such as delayed nucleation and/or rapid phase change dynamics (not considered here) can influence the results to various degrees. Another possible reason for this discrepancy was the actual amount of impurities in the experimental tests which could be slightly different from the listed composition.

The speed of sound in the current model can be tracked as a function of time so its relationship with the decompression wave

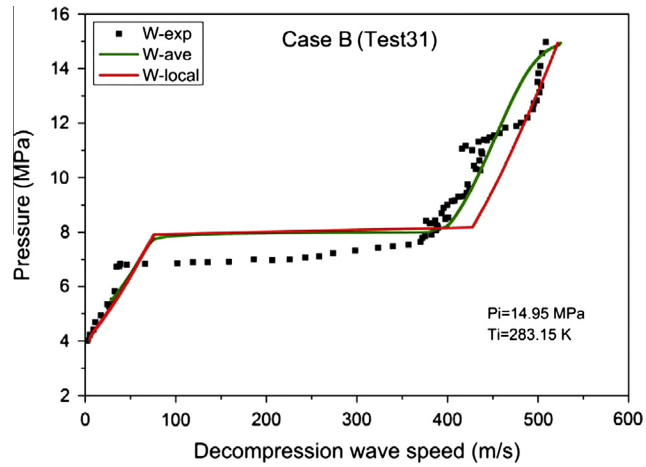


**Fig. 17.** Comparison of the predicted decompression wave speed with the measured results (Case B).

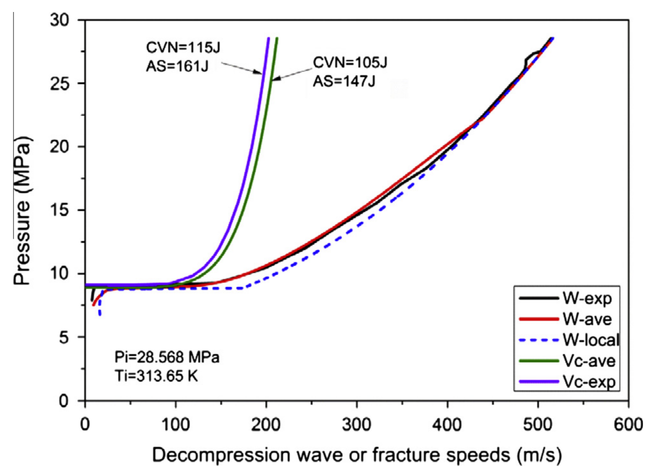


**Fig. 18.** Arrest toughness prediction for Case A.

speed can be clearly understood. For instance, Fig. 17 shows that the 'length' of the pressure plateau (~348 m/s) was almost equal to the sharp drop in the speed of sound due to the phase change, as seen in Fig. 15.

Figs. 10 and 17 show long pressure plateaus that correspond to a significant drop in the decompression wave speed. This would surely influence the ductile fracture propagation control, as outlined in the BTCM. An example is shown in Fig. 18, where the BTCM was used to predict the CVN value of pipe, grade 480 (X70). The diameter and wall thickness of the pipe was 609.6 mm and 19.1 mm respectively. Based on the predicted average decompression wave speed, the corresponding CVN was ~105 J while the CVN value based on the experimentally determined decompression wave speed was ~115 J [56]. The difference between prediction and measurement can be attributed to the difference in the plateau level in the decompression wave speed, because the current CFD model slightly under-predicted the pressure plateau level.

For modern higher grade steels, if the predicted CVN value is greater than ~95 J [57], then the CVN value should be corrected using a certain correction factor to match the results of full-scale burst tests [58,59]. The Australian Standard (AS 2885.1), states that the predicted toughness should be multiplied by a factor of at least 1.4. Fig. 18 shows the decompression wave speed and the fracture propagation speed as functions of pressure. By applying the correction factor, the predicted CVN becomes 147 J whereas the

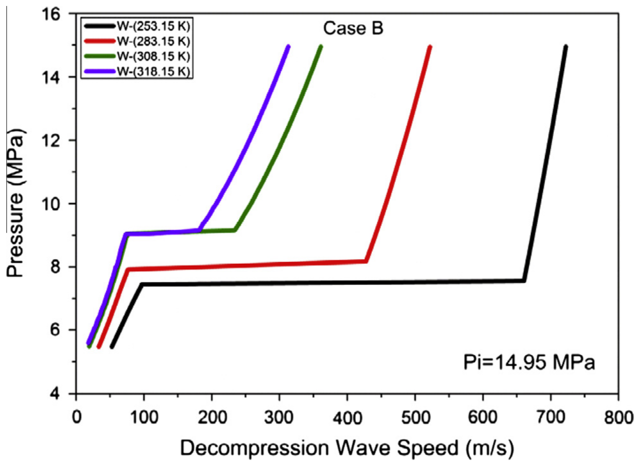


**Fig. 19.** Initial temperature effect on decompression wave speed (Case A).

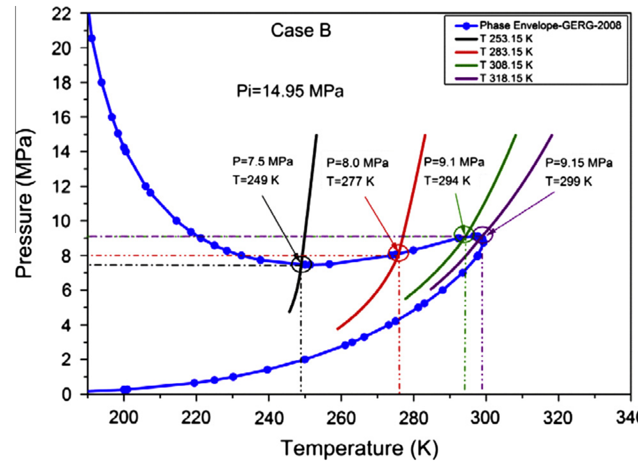


**Fig. 20.** Intersection points with the phase envelope for different initial temperatures (Case B).

measured value was 161 J. Note that the accuracy of the plateau level in the decompression wave speed was within ±0.1 MPa, the size of the pressure step used in the calculation $W_{ave}$.

The pressure plateau level which represents the consequence of phase change on decompression wave speed is an important aspect in determining the required fracture toughness to suppress ductile fracture propagation, so investigating factors that could be sensitive to accurately predict the plateau in decompression wave speed was essential. Further simulations were performed to discuss the influences of initial temperature and impurities on the decompression of $CO_2$ mixtures.

### 5.1. The effect of initial temperature

The influence of initial temperature on the decompression of $CO_2$ mixture was examined for Case B. Three different initial temperatures (−20, 35 and 45 °C) were used while the initial pressure remained the same as the actual case. These temperatures represent three different phases: liquid, dense liquid and supercritical. Fig. 19 shows how changing the initial temperature affects the decompression wave speed. Because the initial temperature of Case B was 10 °C, the main effect of increasing the initial temperature (i.e. 35 and 45 °C) was decreasing the initial decompression wave speed from 521 to 360 and 312 m/s respectively, but lowering the initial temperature caused the initial decompression wave speed to increase to 722 m/s. Moreover, the length and level of the pressure plateaus were affected due to changing the initial temperature; increasing the initial temperature decreased the length of the plateau in the decompression wave speed, and vice versa. Those observations were consistent with the predicted results of pure $CO_2$ conducted by [60] and for mixtures e.g. [14,56]. However, this effect was different in terms of plateau levels for $CO_2$ mixtures because it depended on the shape of the bubble curve on phase envelope, which in turn depended on the amount and type of impurities in the $CO_2$ mixture.

Increasing the initial temperature to 35 and 45 °C raised the level of plateaus by a value of 1 MPa above the main test. Interestingly, as Fig. 19 shows, the apparent plateaus in these two cases occurred at approximately the same level. This can be further explained by representing the pressure–temperature profiles on the phase envelope of the mixture, as depicted in Fig. 20, but note that the phase change occurred at approximately the same pressure level despite different intercept temperatures with the phase boundary which were clearly due to the effect of impurities that rose up the bubble curve on the phase envelope. Such a situation cannot occur for pure $CO_2$.

**Table 6**
The initial conditions of the predominantly $CO_2$ mixtures.

| Case No. | Mixture components (mol %) | | | | | $P_i$ (MPa) | $T_i$ (K) |
|---|---|---|---|---|---|---|---|
| | $CO_2$ | $H_2$ | $N_2$ | $O_2$ | CO | | |
| Case1 | 95 | 5 | 0 | 0 | 0 | 15 | 283.15 |
| Case2 | 95 | 0 | 5 | 0 | 0 | 15 | 283.15 |
| Case3 | 95 | 0 | 0 | 5 | 0 | 15 | 283.15 |
| Case4 | 95 | 0 | 0 | 0 | 5 | 15 | 283.15 |

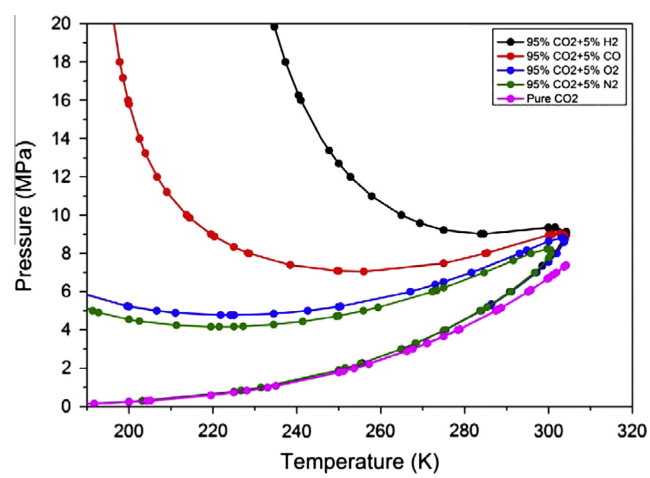


**Fig. 21.** Phase envelope of $CO_2$ mixtures calculated by GERG-2008 EOS.

Where the initial temperature was −20 °C, despite the initial decompression wave speed being much higher than in the main test, the plateau level was predicted at a lower pressure level than the main test by 0.5 MPa. Although this was consistent with the trend in the results of pure $CO_2$ conducted by [60], it cannot be taken as a role for $CO_2$ mixtures because of the shape of the phase boundary. For instance, if the initial temperature was less than (−20 °C), the intersection with the phase boundary would take place at a higher pressure levels because the bubble curve increased again at temperature level below that value. So the trend in the results of pure $CO_2$ which states that as the initial temperature decreases the plateau level in the decompression wave speed decreases cannot be applied for $CO_2$ mixtures.

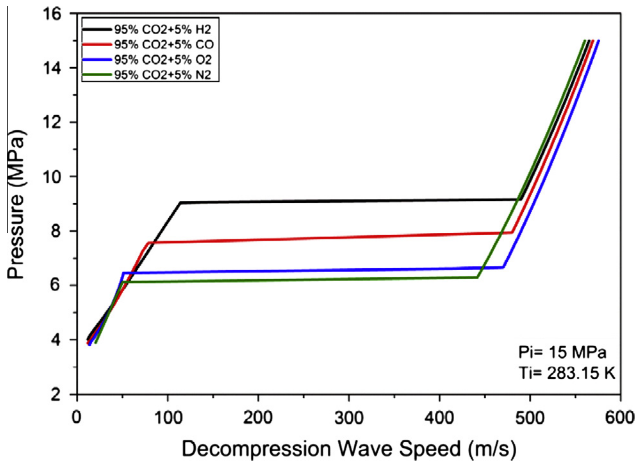


**Fig. 22.** Impurities effect on $CO_2$ decompression wave speed.

### 5.2. Influence of impurities

The effects of several impurities (components other than $CO_2$) on the decompression of $CO_2$ pipelines were examined. The impurities that were most likely to exist in carbon dioxide capture technologies were used [61]. Table 6 lists the four binary $CO_2$ mixtures studied, with the initial conditions.

Fig. 21 illustrates the effect of impurities on the phase envelope of $CO_2$, and show that adding impurities to pure $CO_2$ shifts the critical point and the bubble curve in the phase envelope. Notably, an addition 5% of hydrogen to the $CO_2$ had more effect on the phase equilibrium than the other impurities because it shifted the critical pressure to a value close to 10 MPa.

Simulations of decompression with these binary mixtures were conducted using the same flow domain as in Case A. Fig. 22 shows the influence on the decompression wave speed such that at the same initial conditions and for a fixed fraction of $CO_2$, each impurity resulted in a different initial decompression wave speed and different pressure plateau level that was clearly related to the phase envelope of the mixture. Adding 5% $H_2$ to the $CO_2$ resulted in the highest pressure plateau level ($\sim$9 MPa). Adding 5% $N_2$ resulted in a pressure plateau of about 6 MPa. These changes in the decompression wave speed could influence the fracture propagation/arrest requirements for $CO_2$ pipelines.

## 6. Conclusion

Transporting $CO_2$ mixtures by pipelines is a challenge. In order to improve our knowledge it is important for the modelling tools to handle CCS $CO_2$ mixtures efficiently. The feasibility of complex and possibly large simulations of fluid-pipe interactions, hydraulic transients and dispersion will otherwise be restricted. This paper has described a CFD model developed using ANSYS Fluent to simulate the decompression behaviour of $CO_2$ mixtures. For the first time ever, GERG-2008 EOS was successfully implemented into ANSYS Fluent using UDFs based on an indirect use of the GERG-2008 EOS library. This was done by using pre-compiled thermodynamic property tables ("lookup tables") linked to Fluent during simulation time. Several obstacles related to the EOS library were avoided using this method.

The predicted results were validated against two separate 'shock tube' tests. The results mostly agreed with the experimental results available. The following observations were made:

- The CFD model successfully tracked the rapid drop in pressure and accounted for the phase change during decompression.
- The decompression wave speed curves in $CO_2$ mixtures exhibited long pressure plateaus.
- At the same initial pressure, increasing the initial operating temperature decreases the initial decompression wave speed; and lowering the initial temperature increases the initial decompression wave speed.
- A drop in the initial temperature did not always result in a lower pressure plateau level for $CO_2$ mixtures.
- The existence of hydrogen in $CO_2$ stream had a maximum impact on decompression, compared to the other impurities tested; CO, $O_2$, and $N_2$.

Overall, the current work shows that the CFD technique can be used to predict rapid and severe gas decompression by solving the governing flow equations, in conjunction with the GERG-2008 EOS. This is an effective tool for determining the decompression wave speeds for several $CO_2$-based mixtures and it is also applicable in two- or three-dimensional geometries so the effect of pipe diameter, surface roughness and the shape of fracture outlet can be investigated. The implementation of GERG-2008 allows modelling the real behaviour of $CO_2$ mixture under failure events. This brought about the possibility of using the CFD to investigate several areas related CCS (i.e. the dispersion of $CO_2$).

Future work will focus on developing a 3D decompression model so the effects of pipe opening and the pressure drop behind the crack tip can be identified. A 3D coupled fracture-decompression model is also a target to understand the interaction between the fracturing pipe and decompressing fluid.

## Acknowledgements

This work was funded by the Energy Pipelines CRC, supported through the Australian Government's Cooperative Research Centre Program, and co-funded by the Department of Resources, Energy and Tourism (DRET). The funding and in-kind support from the APIA RSC is gratefully acknowledged.

## References

[1] IE. Building essential infrastructure for carbon capture and storage. Melbourne: Insight Economics Pty Ltd (IE); 2011. p. 43.
[2] Li H, Yan J. Evaluating cubic equations of state for calculation of vapor–liquid equilibrium of $CO_2$ and $CO_2$-mixtures for $CO_2$ capture and storage processes. Appl Energy 2009;86(6):826–36.
[3] Metz B, Davidson O, Coninck Hd, Loos M, Meyer L. IPCC special report on carbon dioxide capture and storage. New York: Intergovernmental Panel on Climate Change; 2005. p. 443.
[4] Zhang Y, Ji X, Lu X. Energy consumption analysis for $CO_2$ separation from gas mixtures. Appl Energy 2014;130:237–43.
[5] IEA, $CO_2$ pipeline infrastructure: an analysis of global challenges and opportunities. International Energy Agency Greenhouse Gas Programme; 2010. p. 1–134.
[6] DNV. Recommended practice DNV-RP-J202 "Design and Operating of $CO_2$ Pipelines"; 2010.
[7] Cosham A, Eiber RJ. Fracture propagation in $CO_2$ pipelines. J Pipeline Eng 2008;4:281–91.
[8] Li H, Yan J. Impacts of equations of state (EOS) and impurities on the volume calculation of $CO_2$ mixtures in the applications of $CO_2$ capture and storage (CCS) processes. Appl Energy 2009;86(12):2760–70.
[9] Maxey WA, Kiefner JF, Eiber RJ. Ductile fracture arrest in gas pipelines. Related Information: A. G. A. Cat. No. L32176. Medium: X; Size; 1976. Pages: 46.
[10] Kiefner JF, Maxey WA, Eiber RJ, Duffy AR. Failure stress levels of flaws in pressurized cylinders progress in flaw growth and fracture toughness testing, ASTM STP 536, American Society for Testing and Materials; 1973. p. 461–81.
[11] Rothwell AB. Fracture propagation control for gas pipelines––past, present and future. In: Denys R, editor. Proceedings of the 3rd international pipeline technology conference. vol. 1; 2000. p. 387–405.
[12] Eiber R, Bubenik T, Maxey W. GASDECOM, computer code for the calculation of gas decompression speed that is included in fracture control technology for natural gas pipelines. NG-18 Report 208. American Gas Association Catalog; 1993.

[13] Starling KE, Powers JE. Enthalpy of mixtures by modified BWR equation. Ind Eng Chem Fundam 1970;9(4):531–7.
[14] Cosham A, Eiber RJ, Clark EB. GASDECOM: carbon dioxide and other components. ASME Conf Proc 2010;2:777–94.
[15] Hopke SW, Lin CJ. Application of BWRS equation to natural gas systems. In: 76'h National AIChE meeting, American Institute of Chemical Engineers, Tulsa, Oklahoma, USA; 1974.
[16] Phillips AG, Robinson CG. Gas decompression behavior following the rupture of high pressure pipelines – Phase 1, PRCI Contract PR-273-0135. Pipeline Research Council International, Inc.; 2002. p. 1–52.
[17] Cosham A, Jones DG, Armstrong K, Allason D, Barnett J. The decompression behaviour of carbon dioxide in the densephase. In: Proceedings of the 2012 9th international pipeline conference. Calgary, Alberta, Canada: ASME; 2012.
[18] Lemmon EW, Huber ML, McLinden MO. NIST standard reference database 23: Reference Fluid Thermodynamic and Transport Properties-REFPROP. Gaithersburg: National Institute of Standards and Technology; 2010.
[19] Span R, Wagner W. A new equation of state for carbon dioxide covering the fluid region from the triple-point temperature to 1100 K at pressures up to 800 MPa. ISSN 1996;25(6):1509–96.
[20] Kunz O, Klimeek R, Wagner W, Jaeschke M. The GERG-2004 wide-range equation of state for natural gases and other mixtures-GERG Technical Monograph 15. Groupe Européen de Recherches Gazières; 2007.
[21] Picard DJ, Bishnoi PR. The Importance of real-fluid behavior and nonisentropic effects in modeling decompression characteristics of pipeline fluids for application in ductile fracture propagation analysis. Can J Chem Eng 1988;66(1):3–12.
[22] Picard DJ, Bishnoi PR. The importance of real-fluid behavior in predicting release rates resulting from high-pressure sour-gas pipeline ruptures. Can J Chem Eng 1989;67(1):3–9.
[23] Mahgerefteh H, Brown S, Denton G. Modelling the impact of stream impurities on ductile fractures in $CO_2$ pipelines. Chem Eng Sci 2012;74:200–10.
[24] Mahgerefteh H, Brown S, Martynov S. A study of the effects of friction, heat transfer, and stream impurities on the decompression behavior in $CO_2$ pipelines. Greenhouse Gases: Sci Technol 2012;2(5):369–79.
[25] Jie HE, Xu BP, Wen JX, Cooper R, Barnett J. Predicting the decompression characteristics of carbon dioxide using computational fluid dynamics. In: Proceedings of the 2012 9th international pipeline conference. Calgary, Alberta, Canada ASME; 2012.
[26] Lu C, Michal G, Elshahomi A, Godbole A, Venton P, Botros KK, et al. Investigating the effects of pipe wall roughness and pipe diameter on the decompression wave speed in natural gas pipelines. In: 9th international pipeline conference 2012. Calgary, Alberta, Canada: ASME; 2012.
[27] Botros KK, Carlson L, Reed M. Extension of the semi-empirical correlation for the effects of pipe diameter and internal surface roughness on the decompression wave speed to include High Heating Value Processed Gas mixtures. Int J Press Vessels Pip 2013;107:12–7.
[28] Botros KK, Geerligs J, Fletcher L, Rothwell B, Venton P, Carlson L. Effects of pipe internal surface roughness on decompression wave speed in natural gas mixtures. ASME Conf Proc 2010;44212:907–22.
[29] Botros KK, Rothwell B, Carlson L, Venton P. Semi-empirical correlation to quantify the effects of pipe diameter and internal surface roughness on the decompression wave speed in natural gas mixtures in 9th international pipeline conference IPC2012. Calgary, Alberta, Canada: ASME; 2012.
[30] Chen JR, Richardson SM, Saville G. Modelling of two-phase blowdown from pipelines—II. A simplified numerical method for multi-component mixtures. Chem Eng Sci 1995;50(13):2173–87.
[31] Bendiksen KH, Maines D, Moe R, Nuland S. The dynamic two-fluid model OLGA: theory and application. SPE Prod Eng 1991;6(2):171–80.
[32] Zucrow MJ, Hoffman JD. Gas dynamics. New York: John Wiley & Sons; 1976.
[33] Mahgerefteh H, Oke A, Atti O. Modelling outflow following rupture in pipeline networks. Chem Eng Sci 2006;61(6):1811–8.
[34] Mahgerefteh H, Saha Pratik, Economou IG. Fast numerical simulation for bore rupture of pressurized pipelines. Am Inst Chem Eng. AIChE J 1999;45(6). 1191–1191.
[35] Brown SF. CFD modelling of outflow and ductile fracture propagation in pressurised pipelines. London: Department of Chemical Engineering, University College London; 2011. p. 227.
[36] Peng D-Y, Robinson DB. A new two-constant equation of state. Ind Eng Chem Fundam 1976;15(1):59–64.
[37] Starling KE, Savidge JL. Compressibility factors of natural gas and other related hydrocarbon gases. american gas association, transmission measurement committee Report No.8, and American Petroleum Institute, MPMS Chapter 14.2 Second Edition); 1994.
[38] Picard DJ, Bishnoi PR. Calculation of the thermodynamic sound velocity in two-phase multicomponent fluids. Int J Multiph Flow 1987;13(3):295–308.
[39] Li H, Jakobsen JP, Wilhelmsen Ø, Yan J. PVTxy properties of $CO_2$ mixtures relevant for $CO_2$ capture, transport and storage: review of available experimental data and theoretical models. Appl Energy 2011;88(11):3567–79.
[40] Patel NC, Teja AS. A new cubic equation of state for fluids and fluid mixtures. Chem Eng Sci 1982;37(3):463–73.
[41] Redlich O, Kwong JNS. On the thermodynamics of solutions. V. An equation of state. Fugacities of gaseous solutions. Chem Rev 1949;44(1):233–44.
[42] Soave G. Equilibrium constants from a modified Redlich-Kwong equation of state. Chem Eng Sci 1972;27(6):1197–203.
[43] Péneloux A, Rauzy E, Fréze R. A consistent correction for Redlich-Kwong-Soave volumes. Fluid Phase Equilib 1982;8(1):7–23.
[44] Hu J, Duan Z, Zhu C, Chou I. PVTx properties of the $CO_2$–$H_2O$ and $CO_2$–$H_2O$–NaCl systems below 647 K: assessment of experimental data and thermodynamic models. Chem Geol 2006;238:249–67.
[45] Yu J-M, Lu BCY, Iwai Y. Simultaneous calculations of VLE and saturated liquid and vapor volumes by means of a 3P1T cubic EOS. Fluid Phase Equilib 1987;37:207–22.
[46] Ji W-R, Lempe DA. Density improvement of the SRK equation of state. Fluid Phase Equilib 1997;130(1–2):49–63.
[47] Liu X, Godbole A, Lu C, Michal G, Venton P. Source strength and dispersion of $CO_2$ releases from high-pressure pipelines: CFD model using real gas equation of state. Appl Energy 2014;126:56–68.
[48] Botros KK. Performance of five equations of state for the prediction of vle and densities of natural gas mixtures in the dense phase region. Chem Eng Commun 2002;189(2):151–72.
[49] Botros KK. Measurements of speed of sound in lean and rich natural gas mixtures at pressures up to 37 MPa using a specialized rupture tube. Int J Thermophys 2010;31(11):2086–102.
[50] Luo X, Wang M, Oko E, Okezue C. Simulation-based techno-economic evaluation for optimal design of $CO_2$ transport pipeline network. Appl Energy 2014;132:610–20.
[51] Liou MS. A new flux splitting scheme. J Comput Phys 1993;107(1):23–39.
[52] Wagner W. Description of the software package for the calculation of thermodynamic properties from the GERG-2004 XT08 wide-range equation of state for natural gases and other mixtures. Ruhr-Universität Bochum; 2009. p. 76.
[53] Wagner W. Description of the software package for the calculation of thermodynamic properties from the GERG-2004 XT08 wide-range equation of state for natural gases and other mixtures. Ruhr-Universitat Bochum; 2009. p. 76.
[54] Andresen T, Skaugen G. Lookup tables based on Gibb's free energy for quick and accurate calculation of thermodynamic properties for $CO_2$. In: 22nd international congress of refrigeration: refrigeration creates the future. Beijing: International Institute of Refrigeration; 2007.
[55] Mahgerefteh H, Atti O, Denton G. An interpolation technique for rapid CFD simulation of turbulent two-phase flows. Process Saf Environ Prot 2007;85(1):45–50.
[56] Botros KK, Hippert Jr E, Craidy P. Measuring decompression wave speed in $CO_2$ mixtures by a shock tube. Pipelines Int 2013;16.
[57] Leis BN, Zhu X-K, Forte TP. New approach to assess running fracture arrest in pipelines. In: Pipeline technology conference, 12–14 October, Ostend, Belgium; 2009.
[58] Hashemi SH. Correction factors for safe performance of API X65 pipeline steel. Int J Press Vessels Pip 2009;86(8):533–40.
[59] Wilkowski G, Rudland D, Xu H, Sanderson N. Effect of grade on ductile fracture arrest criteria for gas pipelines. In: 2006 international pipeline conference. ASME, Calgary, Alberta, Canada, September 25–29; 2006.
[60] Cosham A. $CO_2$: ''It's a gas, Jim, but not as we Know it''. Pipeline Technol Conf 2009:1–16.
[61] Seevam PN, Race JM, Downie MJ, Hopkins P. Transporting the next generation of $CO_2$ for carbon, capture and storage: the impact of impurities on supercritical $CO_2$ pipelines. ASME Conf Proc 2008;48579:39–51.